Performance evaluation of seismic strengthened irregular RC steel hybrid frames

Performance evaluation of seismic strengthened irregular RC-steel hybrid frames

Xiaoge Ren[1]; Shunfeng Gong[2]; and Yong Lu, F.ASCE[3]

[1]Ph.D. Student, Dept. of Civil Engineering, Zhejiang Univ., Hangzhou 310058, China. E-mail:sugar126@zju.edu.cn

[2]Professor, Dept. of Civil Engineering, Zhejiang Univ., Hangzhou 310058, China (Corresponding author). E-mail:sfgong@zju.edu.cn

[3]Professor, School of Engineering, Institute for Infrastructure and Environment, Univ. of Edinburgh, Edinburgh EH9 3JL, U.K. E-mail: yong.lu@ed.ac.uk

Abstract: New carbon-emission requirements have brought about high demand on retrofitting and strengthening of structures in power-generation plants to accommodate installation of pollution control devices. A typical form of the retrofitted structure is a hybrid reinforced concrete (RC)-steel frame with specific irregularity features. This paper presents the seismic performance evaluation of a representative irregular RC-steel hybrid frame formed by a vertical combination of newly added steel frame and a pre-existing RC frame. The prototype structure originates from a real retrofitting project, and the evaluation is carried out numerically by creating six variants of the hybrid frame retrofitted with different strengthening strategies on the RC frame using nonlinear finite element modelling. The seismic performance of hybrid frame structures is comparatively assessed in terms of roof displacement, story drift ratio, residual displacement and hysteretic energy ratio when subjected to a group of selected earthquake ground motions at different intensity levels. Results show that among the three main types of retrofitting schemes, strengthening the pre-existing RC frame with shear walls appears to be most effective in limiting the roof and inter-story drifts. Strengthening the pre-existing RC frames at the local member level tends to be least effective. Overall, retrofitting the hybrid structure with steel bracings is deemed to be a more robust solution, both in terms of controlling the displacements and enhancing the hysteretic energy dissipation capacity.

Author keywords: seismic performance evaluation; irregular hybrid frame; dynamic time-history; strengthening strategy

Introduction

New carbon-emission requirements have brought about high demand on implementing denitrification device in power-generation plants to reduce emission of sulphur dioxide and nitrogen oxide. In consideration of the factors such as economic cost and construction period, retrofitting and strengthening of the pre-existing structure to accommodate installation of pollution control devices tends to be a more attractive option than demolition and re-constructing a new structure. Hybrid form of structures, such as adding a steel frame on top of a pre-existing RC frame, is seemingly a suitable choice to meet the structural extension needs for power-generation plants. At the same time, such extension design also brings about a special type of vertically irregular frame structures, with particular characteristics such as greater variation in strength and stiffness between RC frame and steel frame, and mass concentration on a certain floor, which are not well covered by existing studies on irregular frames.

In the general context of irregularities of structures, many studies have been carried out on the vertical irregularity, and they provided valuable insights into the seismic performance of vertical irregular structures. Tremblay and Poncet (2005) particularly studied the influence of mass irregularity along the height of the structure on the seismic response, and indicated that the mass irregularity conditions had a limited negative impact on the seismic performance of the structures. Based upon inelastic dynamic time-history analysis, Sadashiva et al. (2012) and Zhou et al. (2015) carried out the seismic response of RC structures with vertical strength or stiffness irregularity, respectively, and they pointed out that the vertical strength irregularity and stiffness irregularity have a significant effect on the seismic performance of the structures. Chintanapakdee and Chopra (2004) studied the seismic demands of RC frame structures with strength, stiffness, and strength and stiffness irregularity, and indicated that the effects of combined strength and stiffness irregularity on seismic demands are larger than the two types of irregularity occurring separately. Then, Michalis et al. (2006)

and Nezhad et al. (2015) investigated the effects of four types of irregularity including stiffness, strength, mass, and combined stiffness and strength irregularities along the height of steel frames on the seismic response. These studies concluded that the effects depend not only upon the type and the location of irregularity, but also on the intensity of the earthquake.

Varadharajan et al. (2014a; 2014b) studied various types of vertical irregular RC frames with changes in location and magnitude of irregularity, and proposed equations to estimate the seismic response parameters of irregular RC frames. Lu (2002) pointed out that the distribution of the story shear overstrength is a stable indicator of the general inelastic behaviour of frames. Further, by combining the effects of story stiffness and strength, Lu et al. (2009) introduced a new story capacity factor to evaluate the regularity of frame structures and indicated that the inverse of the story capacity factor correlates well with the story drift distribution. Considering the characteristics of the seismic input, Zhou et al. (2013) carried out a nonlinear dynamic time-history analysis to investigate the effects of vertical irregularities under pulse-type ground motions, and provided a reference modification of ductility reduction factors accounting for vertical irregularities. Lately, Bohlouli and Poursha (2016) performed an eigenvalue analysis to evaluate the dynamic characteristics of steel moment resisting frames with setbacks, and indicated that the location and the degree of setback are two key factors affecting the seismic response of irregular structures.

Two types of irregularity locations have commonly been considered in previous studies, namely structures with setbacks in the upper stories (Athanassiadou 2008; Sarkar et al. 2010) and structures with irregularity located at a certain story, more generally at the first story (Soni and Mistry 2006; Mwafy and Khalifa 2017). Some complex structures with significant irregularities in geometry, mass, and stiffness distributions are investigated as well (Ceci et al 2011; Zhou et al 2014). However, very few studies have been dedicated to the irregularity induced by hybrid structures with a combination of two different frames in elevation. In this study,

71 an irregular hybrid structure with a combination of a newly added steel frame on top of a pre-existing RC
72 frame is investigated. To accommodate the steel frame and withstand the increased loads, several
73 strengthening strategies for retrofitting the RC frame are proposed. Thus, various profiles in terms of the
74 vertical irregularity of the hybrid structures arise, as a result of (1) the difference of configuration and material
75 properties between the steel frame and the RC frame; and (2) different degrees of enhancement in stiffness,
76 strength, and distribution of mass caused by the structural strengthening on the RC frame. The seismic
77 performances of such irregular hybrid frames are comparatively evaluated through the Dynamic History
78 Analysis (DHA) in terms of several structural parameters, and a preferable strengthening strategy is proposed
79 to minimize the negative effect induced by the vertical irregularities.

80 # Representative retrofitted structure and retrofitting schemes

81 *Representative retrofitted structure*

82 For the present study an actual retrofitted structure is employed as a representation of the type of hybrid
83 frame structures. In this case, for the purpose of reducing the atmospheric pollution caused by flue gas
84 emission, a denitrification device named Selective Catalytic Reduction (SCR) reactor and flues needed to be
85 installed to the original power plant RC structure. Because of the limited horizontal space of the surrounding
86 area and the denitrification process requirements, the structure had to be extended upward to support the
87 newly added SCR reactor and flues. Considering the site condition of the boiler and the layout of the
88 denitrification devices, a new steel frame was constructed upon the pre-existing RC frame. Thus, a RC-steel
89 hybrid frame structure with a vertical combination of a RC frame located in lower part and a steel frame
90 located in upper part was generated. In fact, similar installation requirements and space constraints occur in
91 many such power-generation facilities across China, see selected examples in Fig. 1. Therefore, the present
92 case structure can be considered as rather representative.

93 Typical geometric characteristics of the retrofitted hybrid structure and the sizes of primary components
94 are illustrated in Fig.2. The reinforcement details of RC beams and columns are listed in Table 1. The cube
95 compressive strength of concrete is approximately 30 MPa, the yield strengths of longitudinal reinforcement
96 and stirrups are taken as 335 MPa and 235 MPa, respectively. The yield strength of steel columns and beams
97 in the newly-added steel frame is 335 MPa and that of steel bracings is 235MPa.
98 An important consideration in such a retrofitting scheme is that the load-carrying capacity of the pre-
99 existing RC frame has decreased due to strength and stiffness degradation in the previous long period of
100 service. Therefore, the RC frame should be strengthened first to provide necessary enhancement in the
101 structural stiffness and strength before the addition of the upper steel frame. A suitable strengthening strategy
102 should be considered to adequately cover local strengthening of components, strengthening of beam-column
103 joints, and the global structural retrofitting. Therefore, a variety of possible strengthening and retrofitting
104 schemes can arise. This prompts the needs to conduct a systematic evaluation of the seismic performance of
105 hybrid frame structures with various strengthening arrangements, so that comparative results can be
106 generated to assist in the retrofitting design for this category of structures under the framework of
107 performance-based design.
108 *Local strengthening on components*
109 For the existing RC frame, steel plate jacketing was chosen as the local strengthening technique for the
110 beam-column connections, as schematically shown in Fig.3(a). The beam-column joints were jacketed by
111 steel plates of thickness of 12 mm. Four angle steels (∠125×80×12 mm) were bonded to the four corners of
112 the RC beam, and steel batten plates (80×10 mm) spaced at 400 mm were welded to the angle steels to form
113 a steel cage. Epoxy resin adhesive was injected into the gap between angle steels, batten plates and RC beams.
114 An enlargement of the cross section was chosen for strengthening of the RC columns. A concrete layer with

115 higher strength was casted around the existing RC column. A new layer of concrete was reinforced with
116 longitudinal reinforcement according to the strengthening design, and with additional stirrups which were
117 welded to the original stirrups to ensure the integrity of the RC column. The dimensions of column section
118 became 950×950 mm after the strengthening. The strength capacity curves of the RC beams (moment-
119 curvature relationship) and columns (moment-axial force relationship) before and after strengthening are
120 shown in Fig.4.

121 To understand the strengthening effect on the RC frame, especially the performance of the beam-column
122 joint region, a detailed finite element model was created using the software ABAQUS. The FE model and
123 main results are shown in Fig.5. The results confirmed that the load-carrying capacity of RC beams and
124 columns were improved greatly, and no obvious damage was observed within the beam-column joints. Thus,
125 in the main structural analysis using the structural dynamics analysis program PERFORM-3D, which will be
126 described later, the beam-column joints can be treated as rigid, while the strengthened beam and column end
127 regions are modelled as elastic segment with an equivalent elastic flexural rigidity of the strengthened
128 sections.

129 *Global retrofitting approach*

130 For the RC frame part, in addition to the abovementioned member-level strengthening, global
131 strengthening was also considered, and this was achieved by installing either X-pattern steel bracings or
132 concrete shear walls in the two side spans, as shown in Fig.2(b). Steel plates with thickness of 16 mm were
133 used as jackets for the beam-column joints, and steel gusset plates were used to connect the steel bracing and
134 steel plate by welding and bolting, as shown in Fig.3(b). The I-shaped steel bracings were of dimensions
135 200×200×8×12 mm, while the thickness of the concrete shear walls was 200 mm and the ratio of wall
136 reinforcement was 0.9% in the horizontal and vertical directions, respectively. The cube compressive strength

of concrete for the shear walls was approximately 40 MPa, and the yield strengths of longitudinal reinforcement and stirrups were 335 MPa and 300 MPa, respectively. The yield strength of steel bracings and plates was 235 MPa.

Variants of retrofitting scheme and analysis models

In such retrofitted hybrid frames, the newly added steel frame part in the upper story is designed in accordance with the current design requirements. Therefore, the vertical distribution of the story strength and stiffness of the overall hybrid frame is dependent mainly upon the strengthening schemes of the RC frame in the lower stories. To evaluate the regularity features of the strengthened hybrid frames and their effects in the seismic response, six variants of the retrofitted frame are created, as shown in Fig. 6 and explained as follows:

(1) Model A: A basic hybrid structure by simply adding the new steel frame to the top of the pre-existing RC frame.

(2) Model B: A hybrid structure with the pre-existing RC frame strengthened with X-pattern steel bracings in the two side spans.

(3) Model C: A hybrid structure with the pre-existing RC frame strengthened with concrete shear walls.

(4) Model D: A hybrid structure with the components of the pre-existing RC frame strengthened locally.

(5) Model E: A hybrid structure with the pre-existing RC frame strengthened with both X-pattern steel bracings and member strengthening.

(6) Model F: A hybrid structure with the pre-existing RC frame strengthened with both concrete shear walls and member strengthening.

It should be noted that for all the six cases, the newly added steel frame in the upper five stories remain the same. The horizontally braced 6^{th} story within the steel frame was to accommodate the installation of the SCR reactor and the flues. The associated stiffening and mass concentration at this story is another feature

159 of the hybrid structures in terms of the vertical irregularity.

160 Characterisation of vertical irregularity of the hybrid frames

161 The maximum lateral deformation demands, namely the roof displacement and the maximum story drift
162 ratio, are key response parameters in the seismic performance evaluation of structures. These response
163 parameters relate closely to the vertically irregularity for a frame. Such correlation is reflected in many
164 simplified analysis methods. For example, for multi-story buildings responding primarily in the fundamental
165 mode, Miranda (1999) proposed the following formulas for the calculation of the roof displacement, Δ_{roof},
166 and the maximum story drift ratio, $\theta_{\max}$, respectively:

167 $$\Delta_{\text{roof}} = \beta_1 \beta_3 S_d \tag{1}$$

168 $$\theta_{\max} = \beta_2 \beta_4 \frac{\Delta_{\text{roof}}}{H} \tag{2}$$

169 where S_d is the displacement spectrum ordinate corresponding to the fundamental period, H is the
170 height of the building, β_1 is the approximate mode participation factor, β_2 is an amplification factor
171 accounting for the concentrations of interstory drifts, β_3 is the nonlinear amplification factor defined as the
172 ratio of the maximum inelastic displacement to maximum elastic displacement, and β_4 is a factor to
173 represent the intensified concentration of interstory drift due to the nonlinear response. The effects of the
174 vertical regularity are represented through the β_2 and β_4 factors.

175 To characterise the vertical irregularity quantitatively, Lu et al. (2009) proposed a so-called story capacity
176 factor, which represents the combined effect of the story strength and stiffness, and it is defined as:

177 $$i_{\text{sc}} = i_{\text{os}} \times i_{\text{ns}} \tag{3}$$

178 where i_{os} and i_{ns} are story overstrength factor and story stiffness factor, respectively.

179 The story drift distribution is then related to the story capacity by an inversed proportion, i.e. $\beta_i = 1 / i_{\text{sc}}$.
180 Normalizing $\overline{\beta}_i = \beta_i / \beta_{i,\max}$ such that its maximum story drift coefficient equals unity, the story drift can

181 then be calculated as:

182 $$\theta_i = \overline{\beta}_i \theta_{\max} \quad (4)$$

183 Herein the above method using the story capacity factor is adopted to characterise the vertical irregularity,
184 and hence the distribution of story drift, for the six different designs of the hybrid structures. Consider that
185 the design peak ground acceleration was 0.4g, the values of $\overline{\beta}_i$ coefficient for the six hybrid frames are
186 calculated and plotted in Fig. 7.

187 It can be seen first of all that the bracing-stiffened 6th story manifests as a drastic reduction in the relative
188 story drift, such that the corresponding $\overline{\beta}_i$ coefficient is considerably smaller than other stories.

189 Leaving aside the above outlier for the 6th story, the distributions of the $\overline{\beta}_i$ coefficient exhibit distinctive
190 features of the hybrid frame structures retrofitted with different strengthening schemes. For the basic version
191 of the hybrid structure (Model A) without any strengthening of the pre-existing RC frame, the $\overline{\beta}_i$
192 coefficients within the RC frame stories (story 1 to 3) are much larger than those of the steel frame in the
193 upper stories. Similar is the hybrid frame Model D where the RC frame is strengthened only at the member
194 level, although the drift concentration in the lower 3 stories is somewhat improved. In contrast, for the hybrid
195 structures with the pre-existing RC frame being retrofitted with shear walls (Model C and F), the $\overline{\beta}_i$
196 coefficients within the RC frame stories are much smaller than those of the newly added steel frame. By
197 comparison, the hybrid structures (Model B and E) with the pre-existing RC frame being retrofitted with steel
198 bracings show a quite uniform drift distribution. The drift distributions from the $\overline{\beta}_i$ coefficients represent
199 clearly the enhancement degree of stiffness and strength resulted from the structural retrofitting schemes.

200 In order to evaluate more accurately the effect of the different retrofitting schemes on the seismic response
201 of the hybrid structures, and to assess the adequacy of using the story capacity factor in estimating the story
202 drift distribution, dynamic time-history analyses are performed on the six hybrid frames. The detailed

dynamic analysis and the study of the time-history responses of the frames are presented in the following sections.

Seismic response analysis of hybrid frames: structural model and input ground motions

Structural modelling

The structural analysis program PERFORM-3D is used to carry out a nonlinear dynamic time-history response analysis of the six hybrid frame models. The chord rotation model with plastic hinges at the end of a member is selected to simulate both steel and RC beams and columns, as shown in Fig. 8(a), and nonlinear bar elements are used for modelling of steel bracings. The shear wall is simulated by a concrete fiber model with reinforcement details as specified from the design. According to the detailed finite element analysis for the strengthened RC beam-columns as mentioned in the section “Local strengthening on components”, the strengthened end regions of the RC beams and columns are modelled as elastic end zones with an equivalent sectional rigidity. The beam-column joints are treated as rigid, with the sizes of the rigid joint zones being obtained from the actual beam-column connections. In order to satisfy the requirement of the hinge connections at the beam end in the steel frame, a moment release is applied at the end of the steel members which are hinge connected to the RC frame.

A general elastic-plastic and strength degradation model is employed to represent the nonlinear behavior of the individual structural components. The details of the force-deformation relationship are illustrated in Fig.8(b), and it represents the moment-rotation relationship for beams and columns, the axial force-deformation relationship for bracings, respectively. The strength loss of structural components is considered to take into account the generated damages caused by tensile fracture, concrete crushing, concrete shear failure, and steel bracing buckling. The residual strength of RC and steel components is defined according to

225 the strength loss ratio of residual strength to ultimate strength according to FEMA 356 (FEMA 2000). The
226 residual strength ratio of beams, columns and bracing members in compression is defined as 0.2, and that of
227 bracing in tension is defined as 0.8. Furthermore, stiffness and strength degradation of structural components
228 is also taken into account. For the current study, stiffness and strength degradation parameters are defined
229 based on the degradation rule of reversed cyclic loading in Mander's model (Chen et al 2010); the stiffness
230 degradation is defined according to the degradation factor of unloading stiffness as shown in Fig.8(c), while
231 the degradation factor of unloading strength in all regions is taken as 1.0. Geometric nonlinearity, i.e. the *P-*
232 *Δ* effect, is considered in elastic and inelastic dynamic time-history analyses, and a 4% constant modal
233 damping (Papageorgiou and Gantes 2010, 2011) is defined in the seismic response analysis.
234 *Input ground motions*
235 Several procedures have been proposed in the literature to scale the ground motion records (Watson-
236 Lamprey and Abrahamson 2006; Baker 2010; Sextos et al 2011; Kwong et al 2015). Scaling the records to
237 fit a target spectral acceleration S_a with a given range of period T is adopted in the present study. Generally,
238 scaling the records to the target spectrum at the fundamental period (T_1) has been found to be effective to
239 predict the response of first-mode dominated buildings, while for long-period buildings, studies suggested
240 that scaling the records to the target spectrum at a period range between $0.2T_1$ -$1.5T_1$ (ASCE 2010) or $0.2T_1$
241 -$2T_1$ (EC8 2004) was more reasonable.
242 Eight ground motion records as listed in Table 2, obtained from the Pacific Earthquake Engineering
243 Research Center (PEER) Next Generation Attenuation (NGA) strong motion database, are selected based on
244 magnitude and soil classification. The magnitude of these records is in the range of 6.0 to 7.5, and the average
245 shear-wave velocity in the upper 30 m (V_{s30}) is in the range of V_{s30}=250 to 500 m/s to represent the earthquake
246 scenarios with stiff soil class II (classification in Chinese seismic design code).

247 Scaling procedure of the ground motion records to match the target design spectrum is completed using
248 the software SeismoMatch, which is an application capable of adjusting earthquake record through adding
249 wavelets to the acceleration time-history of the selected record to match the target design spectrum (Hancock
250 et al 2006). Based on Eurocode 8 (EC8 2004), the target design spectra as shown in Fig.9 are determined
251 according to primary characteristics such as Peak Ground Acceleration (PGA) of 0.4g, 0.8g, and 1.2g,
252 damping ratio of 5%; and site class. The ground motion records are scaled to match the entire target design
253 spectrum, as shown in Fig.10(a)-(c). In this way, 24 scaled input ground motions are finally employed in the
254 dynamic time-history analyses.

255 ## Seismic response analysis of hybrid frames: results and discussion

256 Basic structural parameters, such as roof displacement, story drift ratio, residual drift ratio, deformation
257 capacity and energy dissipation, are presented and discussed in this section. Eurocode 8 stipulates that the
258 most unfavorable value of the seismic response should be selected if three different seismic records are used
259 in the dynamic time-history analysis; otherwise, the response can be derived from the average value when
260 seven or more different seismic records are used. Thus, the average value of seismic responses from the eight
261 earthquake record analyses is used in this study.

262 *Roof displacement*

263 The roof displacement is a global measure that relates to the structural damage of the frames. The roof
264 displacements for six hybrid structure models resulting from the time-history analysis with PGA=0.4g,
265 PGA=0.8g and PGA=1.2g, respectively, are shown in Fig.11.

266 Compared with the basic hybrid frame Model A, Model B and C with the RC frame being retrofitted with
267 steel bracings and concrete shear walls result in a decrease in roof displacements, and the reduction in Model
268 C is more remarkable than that in Model B. The roof displacement decrease in Model D where the RC frame

269 is strengthened only at the member level is much smaller. These results suggest that steel bracings and
270 concrete shear walls can efficiently reduce the maximum roof displacements of the hybrid frame structure,
271 whereas member level strengthening is less effective. This may be explained by the fact that local
272 strengthening techniques applied on components have limited effect on the improvement of the structural
273 lateral stiffness and the base shear capacity. The same conclusion can be drawn from the comparison on roof
274 displacements between the hybrid structures with pre-existing RC frame being retrofitted with both global
275 and local strengthening techniques and the hybrid structures with pre-existing RC frame being retrofitted
276 with only global strengthening.

277 The roof displacements, Δ_{roof}, are calculated using response spectrum method assuming the response is
278 governed primarily by the fundamental mode. For this purpose, the fundamental period of the six structures
279 are calculated and these are listed in Table 3. The fundamental periods of the hybrid structures with RC frame
280 being retrofitted with either structural-level or member-level strengthening techniques decrease to varying
281 degrees. Included in the table are also the elastic spectral accelerations and displacements for the six
282 structures, and roof displacements calculated according to Eq. (1). Fig.12 compares the roof displacements
283 calculated according to Eq. (1) and the roof displacements attained in the dynamic time-history analysis.

284 As can be seen, the roof displacements calculated by Eq. (1) are almost equal to those obtained from
285 dynamic time-history analysis except for the hybrid frames with pre-existing RC frame being retrofitted with
286 concrete shear wall. This may be explained by the fact that the concrete shear wall increases the degree of
287 vertical irregularity of the hybrid frame; besides, the response of the hybrid frame is also affected by higher
288 mode effects while the mode participation factor of the fundamental mode decreases remarkably.

289 *Story drift ratio*

290 Owing to the vertical irregularity, undesirable failure mechanisms of structures are usually governed by

weak stories. Therefore, the story drift ratio, δ, known as one of the key factors in seismic response of the structure, is analyzed to verify the location of weak stories and the damages along the structural height. The story drift ratios obtained from the dynamic time-history analysis with PGA=0.4g are shown in Fig.13. For a comparison, the story drifts calculated according to Eq. (4) are also shown in the figures.

For the basic version of the hybrid structure (Model A), the distributions of story drift ratios calculated by Eq. (4) and the corresponding $\overline{\beta}_i$ coefficients are almost equal to the story drift ratios obtained from dynamic time-history analysis, as shown in Fig.13. The same conclusion can be drawn for the hybrid structure with RC frame being strengthened only at the member level (Model D) and being retrofitted with steel bracings (Model B and E). For the hybrid structure Model C and F where RC frame is retrofitted with concrete shear wall, the story drift ratios calculated by Eq. (4) are smaller than those obtained from dynamic time-history analysis, but the distribution of corresponding $\overline{\beta}_i$ coefficients is consistent with the vertical distribution of stiffness and strength characteristics in the hybrid frames.

Story drift ratios, δ, for six hybrid structures in different seismic levels are illustrated in Figs.14-16.The story drift ratio of the 6th story is evidently smaller than other stories, and it is consistent with the corresponding $\overline{\beta}_i$ coefficients. For Model A and Model D, the maximum story drift ratios within the pre-existing RC frame on the lower part are much larger than those of the newly added steel frame in the upper part. Thus, the weak stories of Model A and Model D occur in the pre-existing RC frames under strong ground motions. For Model C and Model F, on the contrary, the maximum story drift ratios within the RC frame are smaller than those of the steel frame, which illustrates that the weak stories of Model C and Model F, although not remarkable, are located at the bottom story of steel frame. For Model B and Model E, the maximum story drift ratios are relatively uniform except for the strengthened story, and this suggests that no typical weak story exists in these two models.

313 Based on the above comparisons, the approach using the capacity factor and the corresponding $\overline{\beta}_i$
314 coefficient proves to yield a good indication of the distribution of irregularity along the frame height. It can
315 be observed in Figs.15-16 that retrofitting the RC frame part with global strengthening techniques, including
316 steel bracings and concrete shear walls, can efficiently reduce the story drift ratios and consequently avoid
317 the occurrence of weak story in the pre-existing RC frame. Although concrete shear walls have more positive
318 effect than steel bracings in reducing the story drift ratio, strengthening the RC frame with steel bracings is
319 deemed to be a preferred approach considering the ease of construction. Furthermore, the structure retrofitted
320 with steel bracings possesses a more uniform distribution of story drift ratios.

321 Comparatively, the local strengthening techniques only achieve a limited improvement in the lateral
322 stiffness and base shear capacity of the global frame, and consequently results in a limited reduction of story
323 drift ratios. It should be noted, however, that the improvement effect of this strengthening approach tends to
324 increase with the increase of the seismic ground motion intensity. This is mainly due to the fact that after the
325 structure enters into an advanced level of nonlinear response, the structural components that are improved by
326 local strengthening techniques tend to play an increasingly important role.

327 *Distribution of plastic hinges and failure mechanism*

328 The plastic hinge patterns of the six hybrid structure models under one of the ground motions (Northridge,
329 scaled to PGA=1.2g) are depicted in Fig.17. The plastic hinges in beams and columns are shown using circle
330 marks, and the axial yielding of bracings are shown using oval marks.

331 It can be seen that the inelastic deformation is mainly concentrated in the lower three stories in the basic
332 version of the hybrid structure (Model A) and the hybrid frame which is strengthened only at the member
333 level (Model D), and there is almost no inelastic deformation in the newly added steel frame. Thus, the
334 damage of these two hybrid structures is concentrated in the pre-exiting RC frame, even with the member

335 level strengthening.

336 The concentration of inelastic deformation in the RC frame stories is effectively eliminated in the hybrid
337 structures with the pre-existing RC frame being retrofitted with steel bracings or concrete shear walls. For
338 the hybrid structures with RC frame being strengthened with shear walls (Model C and F), the inelastic
339 deformation is mainly concentrated in the newly added steel frame, and the failure of the hybrid structure is
340 possibly caused by the damage of steel bracings at the bottom story of the steel frame. For the hybrid
341 structures with RC frame being retrofitted with steel bracings (Model B and E), the inelastic deformation is
342 mainly developed in the steel bracings in both RC frame and steel frame stories, while the inelastic
343 deformation in the RC components is avoided due to the member level strengthening.

344 *Distribution of nonlinear hysteretic energy dissipation in primary components*

345 For hybrid frames with vertical irregularity, the evaluation of the hysteretic energy dissipation in primary
346 components provides further insight into the distribution of cumulative damage and possible failure
347 mechanisms. For this purpose, the hysteretic energy dissipation participation factor γ is adopted, which is
348 defined as a proportion of nonlinear hysteretic energy dissipation in a certain component to the total nonlinear
349 hysteretic energy dissipation. Thus, the sum of the hysteretic energy dissipation participation factors of all
350 components in a structure equals to 1. The hysteretic energy dissipation participation factor can be expressed
351 as follows:

352 $$\gamma_i = \frac{EH_i}{EH} \tag{5}$$

353 where γ_i is the hysteretic energy dissipation participation factor of an individual member, for example a
354 steel bracing, a beam or a column.

355 The average values of γ for each type of the primary components in the six models under the ground
356 motions with PGA=1.2g are indicated in Fig.18, in which $\gamma_{\text{beam-c}}$, $\gamma_{\text{column-c}}$, and $\gamma_{\text{bracing-c}}$ are the

hysteretic energy dissipation participation factors of beams, columns, and bracings in the pre-existing RC frame, respectively. $\gamma_{\text{bracing}-\text{s}}$ is the hysteretic energy dissipation participation factor of bracings in the newly added steel frame.

It can be seen from Fig.18 that the energy dissipation is almost totally concentrated in the pre-existing RC frame for Model A and Model D, where the flexural yielding of beams and columns in the RC frame is the primary source of energy dissipation, with beams playing a dominant role. For Model F with the pre-existing RC frame being retrofitted with concrete shear walls, no inelastic deformation occurs in the RC frame, whereas the bracings in the steel frame dissipate almost all seismic energy. The concrete shear walls exhibit hardly any inelastic deformation when the structure is subjected to the strong seismic ground motion.

When the RC frame is retrofitted with steel bracings (Model B and E), the yielding and buckling of steel bracings becomes the main source of the energy dissipation, and at the same time the beams and columns in the RC frame also dissipate an appreciable amount of seismic energy, as can be observed in Fig.18(b) and Fig.18(e). These two cases exhibit a more favorable mechanism of hysteretic energy dissipation, which includes the first lateral-resisting system of steel bracings and the second lateral-resisting system of RC frame. Overall, the hybrid structure with the RC frame being retrofitted with steel bracings and local strengthening techniques achieves a generally uniform distribution of response characteristics along the frame height, and consequently provides a preferable hysteretic energy dissipation capacity in the structural seismic resistance.

Residual roof drift ratio

The residual displacement of a structure system following nonlinear deformation plays an important role in the performance evaluation of the structure, especially in terms of the system stability and repairability. The residual displacements are sensitive to the inelastic mechanism of the system, the hysteretic behavior of structural components, as well as the intensity of the input ground motion; therefore, uncertainty and

379 variability exists in the assessment of the residual displacements.

380 Herein the residual roof displacements of the various hybrid frame models under a strong ground motion
381 are discussed. One of the aforementioned 24 scaled input ground motions (Northridge, PGA=1.2g) is selected
382 to carry out a representative study on residual displacements of the six models, and the roof drift ratio is
383 illustrated in Fig.19. In comparison with the basic version of the hybrid structure (Model A) without any
384 strengthening of the pre-existing RC frame, the residual roof drift ratios of the structures with pre-existing
385 RC frame being retrofitted with either global or local strengthening techniques decrease to some extent. A
386 combination of local and global strengthening techniques on RC frame is more effective in reducing residual
387 roof drift ratio.

388 # Conclusions

389 This paper investigated a special type of irregular hybrid frames arising from retrofitting and extending a
390 pre-existing RC frame with additional stories by a steel frame. The prototype of the hybrid frame was from
391 an actual re-development project. To provide a systematic evaluation of the seismic performance of such
392 hybrid structures, six different strengthening schemes have been considered, resulting in six different hybrid
393 frame structures. These hybrid frames have been analyzed with regard to their irregularity characteristics and
394 the distribution and magnitude of the seismic responses, and the comparative results are examined in order
395 to identify more favorable strengthening schemes especially on the pre-existing RC frame. The following
396 conclusions can be drawn:

397 (1) The story capacity factor and the corresponding story drift distribution coefficients ($\overline{\beta}_i$) are observed
398 to represent well the degree of stiffness and strength enhancement resulting from the structural
399 retrofitting schemes, as well as the actual distribution of story drifts comparing with the time history
400 analysis results.

(2) The hybrid structures with RC frame being retrofitted with either steel bracings or concrete shear walls prove to be most effective in reducing the maximum roof displacement. On the contrary, the hybrid structures where the RC frame is strengthened only at the member level appears to be least effective in reducing the roof displacement. This can be attributed to the fact that the local strengthening techniques applied on the RC components generally lead to only a limited enhancement on the overall lateral stiffness and the base shear capacity.

(3) Nevertheless, the hybrid frame structure with RC frame being retrofitted with only local strengthening techniques exhibits a favorable response mechanism with a strong-column and weak-beam characteristic. The hybrid structure where RC frame is strengthened with steel bracings exhibits a dual lateral-resisting system with a good energy dissipation capacity in the structural seismic resistance. On the other hand, the hybrid frame structure with the RC frame being strengthened by concrete shear walls does not perform well in terms of the energy dissipation in the strengthened hybrid frame structure.

(4) The residual roof displacement of the hybrid frame structure with pre-existing RC frame being retrofitted with either global or local strengthening techniques decreases in comparison with the basic version of the hybrid structure, while the combination of local and global retrofitting techniques is more effective in reducing the residual roof displacement.

In summary, while using concrete shear walls in retrofitting the pre-existing RC frame provides remarkable effect on reducing the roof displacement and the story drift ratios, installing steel bracings along the two side bays is deemed to provide a more robust solution in terms of a more uniform distribution of story drift ratios and avoidance of weak stories. Such a scheme also enables a dual lateral-resisting system with good hysteretic energy dissipation capacity in the structural seismic resistance.

Acknowledgement

423 The authors acknowledge the supports from the Zhejiang Province Key Research and Development
424 Program (Grant number 2018C03033-1) and the National Natural Science Foundation of China (Grant
425 numbers 51779223, 51479176, 51009122) for this study.

426 References

427 ASCE. (2010). "Minimum design loads for buildings and other structures." Reston, VA.

428 Athanassiadou, C. J. (2008). "Seismic performance of R/C plane frames irregular in elevation." *Eng. Struct.*,
429 30(5):1250-1261.

430 Baker, J. W. (2010). "Conditional mean spectrum: Tool for ground-motion selection." *J. Struct. Eng*.,
431 10.1061/(ASCE)ST.1943-541X.0000215.

432 Bohlouli, Z., and Poursha, M. (2016). "Seismic evaluation of geometrically irregular steel moment resisting
433 frames with setbacks considering their dynamic characteristics." *Bull. Earthquake Eng*., 14(10):2757-2777.

434 Ceci, A. M., Gattulli, V., and Potenza, F. (2011). "Serviceability and damage scenario in irregular RC
435 structures: post-earthquake observations and modeling predictions." *J. Perform. Constr. Facil.*,
436 10.1061/(ASCE)CF.1943-5509.0000317, 98-115.

437 Chen, X. W., Li, J. X., and Cheang, J. (2010). "Seismic performance analysis of Wenchuan Hospital structure
438 with viscous dampers." *Struct. Des. Tall Spec. Build.*, 19(4): 397-419.

439 Chintanapakdee, C., and Chopra, A. K. (2004). "Seismic response of vertically irregular frames: response
440 history and modal pushover analyses." *J. Struct. Eng*., 10.1061/(ASCE)0733-9445(2004)130:8(1177).

441 Eurocode 8. (2004). "Design of Structures for earthquake resistance–Part 1: General rules, seismic actions
442 and rules for buildings." Brussels, Belgium.

443 FEMA-356. (2000). "Prestandard and commentary for the seismic rehabilitation of buildings." Washington
444 DC, USA.

445 Hancock, J., Watson-Lamprey, J., Abrahamson, N. A., Bommer, J. J., Markatis, A., Mccoy, E., and Mendis,
446 R. (2006). "An improved method of matching response spectra of recorded earthquake ground motion
447 using wavelets." *J. Earthquake Eng.* 10(spec01): 67-89.
448 Kwong, N. S., Chopra, A. K., and McGuire, R. K. (2015). "Evaluation of ground motion selection and
449 modification procedures using synthetic ground motions." *Earthquake Eng. Struct Dyn.*, 44(11):1841-
450 1861.
451 Lu, Y. (2002). "Comparative study of seismic behavior of multistory reinforced concrete framed structures."
452 *J. Struct. Eng*., 10.1061/(ASCE)0733-9445(2002)128:2(169).
453 Lu, Y., Gu, X. M., and Wei, J. W. (2009). "Prediction of seismic drifts in multi-story frames with a new story
454 capacity factor." *Eng. Struct.*, 31(2): 345-357.
455 Michalis, F., Dimitrios, V., and Manolis, P. (2006). "Evaluation of the influence of vertical irregularities on
456 the seismic performance of a nine-story steel frame." *Earthquake Eng. Struct Dyn.*, 35(12):1489-1509.
457 Miranda, E. (1999). "Approximate seismic lateral deformation demands in multistory buildings." *J. Struct.*
458 *Eng*., 10.1061/(ASCE)0733-9445(1999)125:4(417).
459 Mwafy, A., and Khalifa, S. (2017). "Effect of vertical structural irregularity on seismic design of tall
460 buildings." *Struct. Des. Tall Spec. Build.*, DOI: 10.1002/tal.1399.
461 Nezhad, M. E., and Poursha, M. (2015). "Seismic evaluation of vertically irregular building frames with
462 stiffness, strength, combined-stiffness-and-strength and mass irregularities." *Earthquakes Struct.*, 9(2):
463 353-373.
464 Papageorgiou, A. V., Gantes, C. J. (2010). "Equivalent modal damping ratios for concrete/steel mixed
465 structures." *Comput. Struct.*, 88(19-20):1124-36.
466 Papageorgiou, A. V., Gantes, C. J. (2011) "Equivalent uniform damping ratios for linear irregularly damped

concrete/steel mixed structures." *Soil Dyn. Earthquake Eng*., 31(3):418-30.

Sadashiva, V. K., MacRae, G. A., and Deam, B. L. (2012). "Seismic response of structures with coupled vertical stiffness–strength irregularities." *Earthquake Eng. Struct Dyn.*, 41(1):119-138.

Sarkar, P., Prasad, A. M., and Menon, D. (2010). "Vertical geometric irregularity in stepped building frames." *Eng. Struct.*, 32(8):2175-2182.

SeismoMatch [Computer software]. Seismosoft, Pavia, Italy.

Sextos, A. G., Katsanos, E. I., and Manolis, G. D. (2011). "EC8-based earthquake record selection procedure evaluation: Validation study based on observed damage of an irregular R/C building." *Soil Dyn. Earthquake Eng*., 31(4):583-597.

Soni, D. P., and Mistry, B. B. (2006). "Qualitative review of seismic response of vertically irregular building frames." *ISET J. Earthquake Technol.*, 43(4): 121-132.

Tremblay, R., and Poncet, L. (2005). "Seismic performance of concentrically braced steel frames in multistory buildings with mass irregularity." *J. Struct. Eng*., 10.1061/(ASCE)0733-9445(2005)131:9(1363).

Varadharajan, S., Sehgal, V. K., and Saini, B. (2014a). "Seismic behavior of multistory RC building frames with vertical setback irregularity." *Struct. Des. Tall Spec. Build.*, 23(18):1345-1380.

Varadharajan, S., Sehgal, V. K., and Saini, B. (2014b). "Seismic response of multistory reinforced concrete frame with vertical mass and stiffness irregularities." *Struct. Des. Tall Spec. Build.*, 23(5):362-389.

Watson-Lamprey, J., and Abrahamson, N. "Selection of ground motion time series and limits on scaling." *Soil Dyn. Earthquake Eng*., 26(5):477-482.

Zhou, J., Bu, G., Wang, H., and Cai, J. (2013). "Modification of Ductility Reduction Factor for Vertically Irregular Structures Subjected to Pulse-Like Ground Motions." *Adv. Struct. Eng.*, 16(4):641-652.

489 Zhou, J., Zhao, W., and Mao, W. (2015). “Least Favorable Probability of Failure for 5-and 10-story RC Frame
490 Structures with Vertical Irregularities.” *J. Earthquake Eng.*, 19(7):1158-1180.
491 Zhou, L., Ni, C., Chui, Y. H., and Chen, Z. (2014). “Seismic Performance of a Hybrid Building System
492 Consisting of a Light Wood Frame Structure and a Reinforced Masonry Core.” *J. Perform. Constr. Facil.*,
493 10.1061/(ASCE)CF.1943-5509.0000597, A4014013.

Table 1. Details of RC beams and columns

Component	Size(mm)	Longitudinal reinforcement	Stirrup
Beam-1	400×600	4Φ25+4Φ25	Φ8@100/200
Beam-2	400×800	6Φ25+4Φ25	Φ8@100/200
Column	650×650	4Φ28+16Φ25	Φ10@100

Table 2. Eight ground motion records used in analysis

Number	Earthquake	Year	Station name	Magnitude	V_{s30} (m/s)	PGA (g)
1	Duzce	1999	Duzce	7.14	281.86	0.4043
2	Imperial Valley	1995	Shin-Osaka	6.90	256.00	0.2333
3	Kobe	1979	Coachella Canal #4	6.53	336.49	0.1280
4	Loma Prieta	1989	Gilroy Array #3	6.93	349.85	0.5399
5	Morgan Hill	1984	Gilroy Array #2	6.19	270.84	0.2129
6	Northridge	1994	Leona Valley #2	6.69	435.64	0.0633
7	Parkfield	1966	Cholema-Shandon Array #12	6.19	408.93	0.0597
8	Victoria	1980	SAHOP Casa Flores	6.33	338.60	0.0690

Table 3. Calculated parameters of response spectrum method

Models	T (s)	S_a (g)	S_d (mm)	Δ_{roof} (mm)
Model A	0.552	1.15	86.98	75.97
Model B	0.420	1.15	50.36	38.17
Model C	0.353	1.15	35.57	18.22
Model D	0.499	1.15	71.08	59.54
Model E	0.393	1.15	44.09	34.18
Model F	0.319	1.15	29.05	13.94

(a) 

(b) 

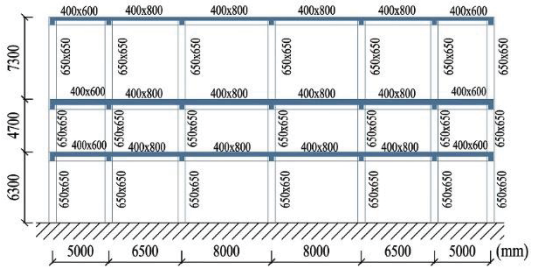

(a)

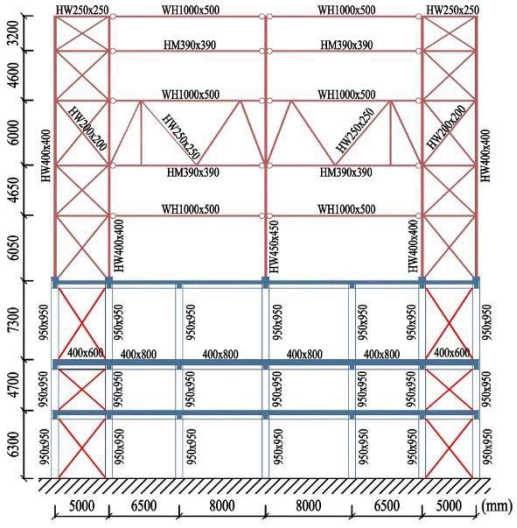

(b)

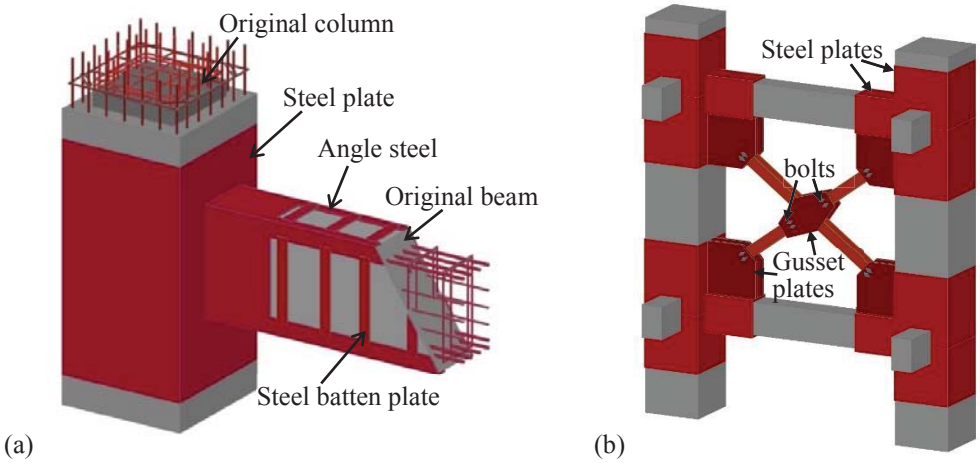

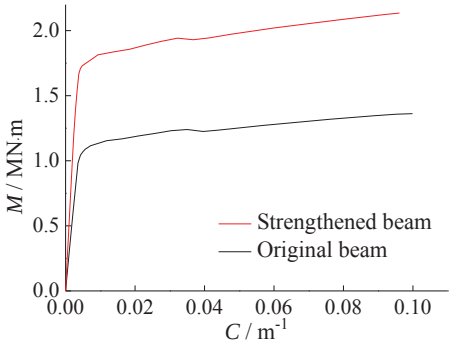

(a)

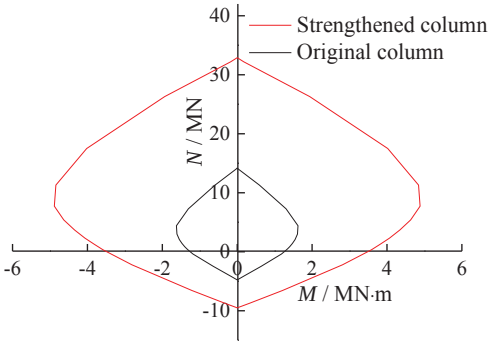

(b)

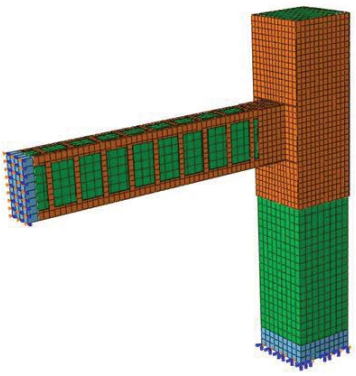

(a)

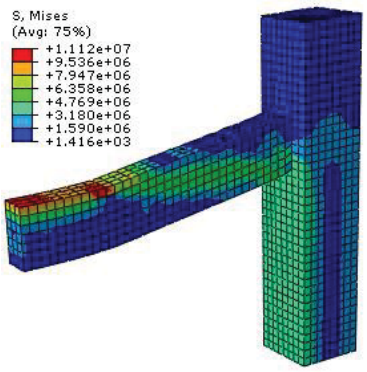

(b)

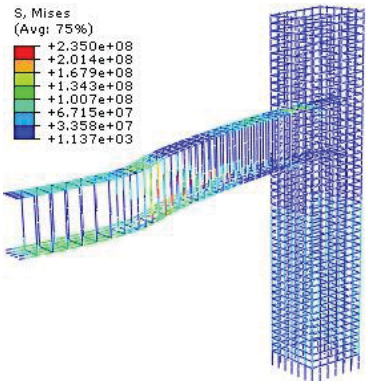

(c)

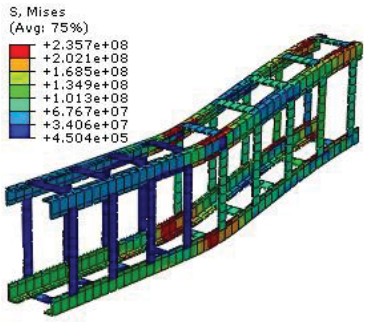

(d)

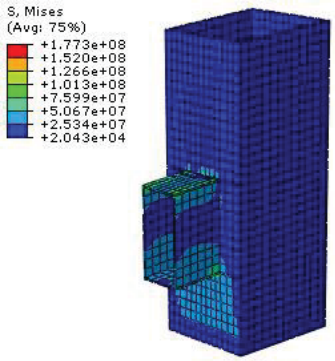

(e)

Fig 6

Click here to download Figure Fig 6.pdf

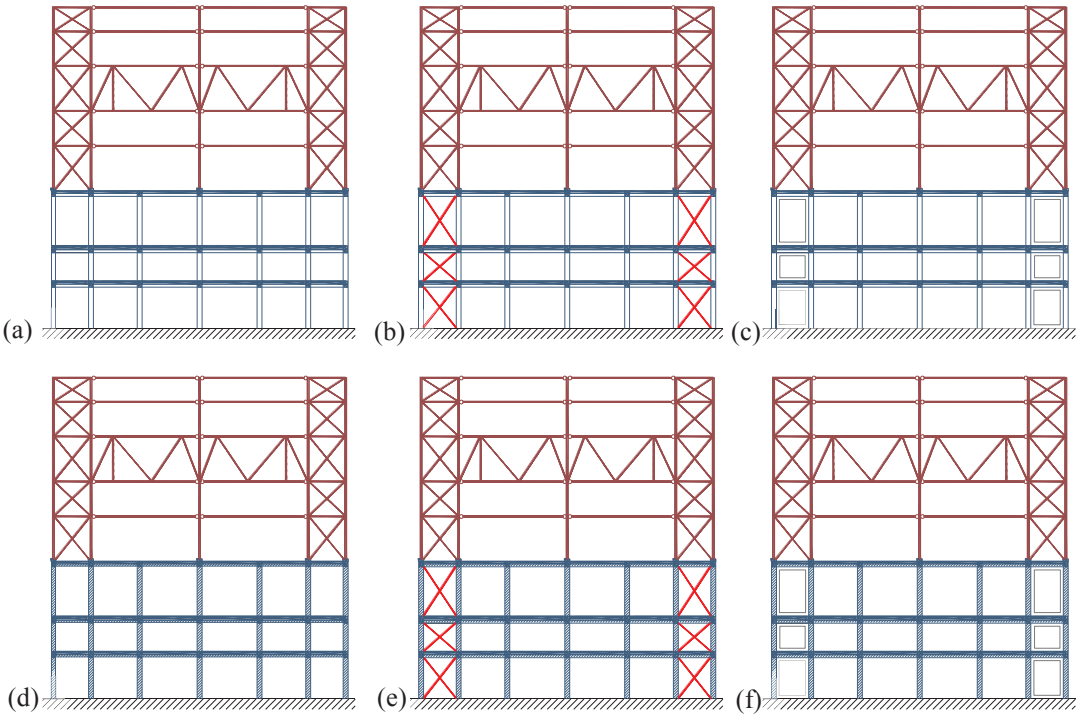

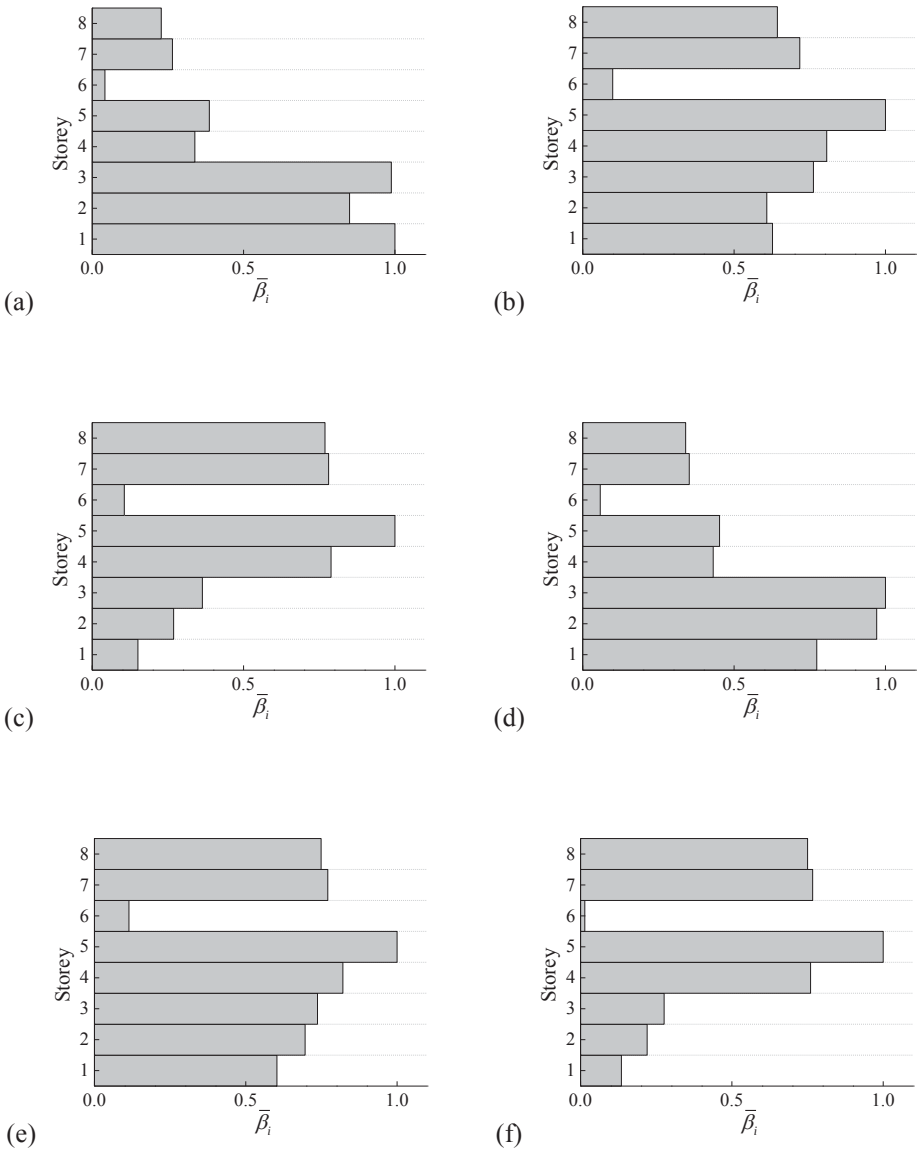

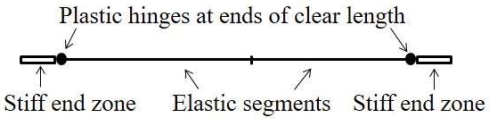

(a)

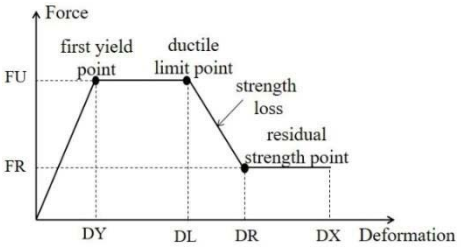

(b)

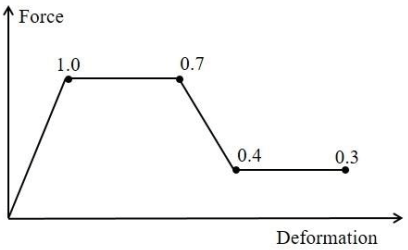

(c)

Fig 9

Click here to download Figure Fig 9.pdf

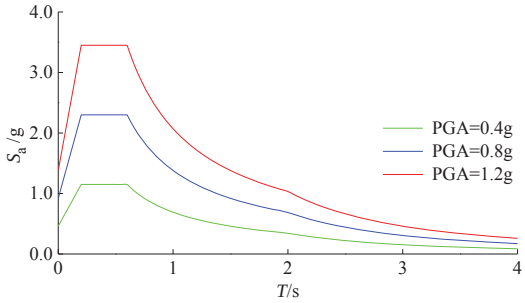

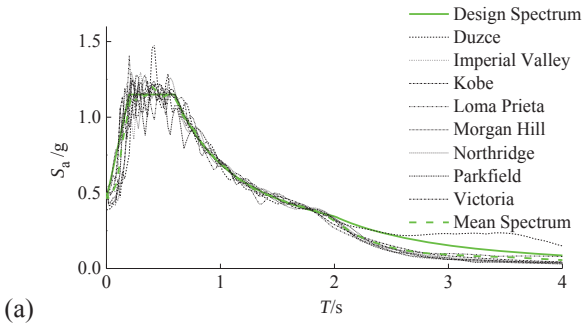

(a)

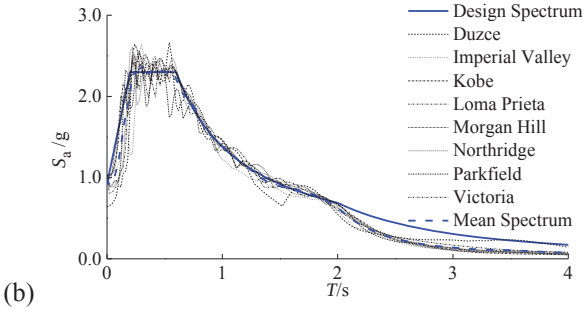

(b)

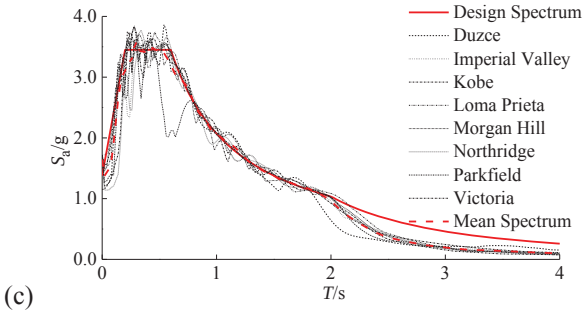

(c)

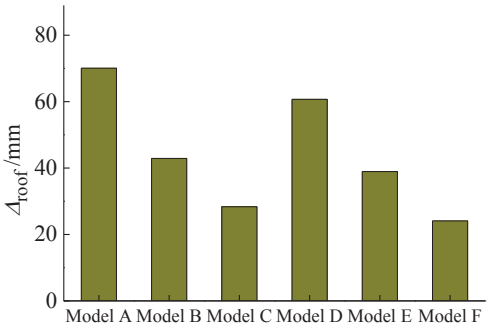

(a)

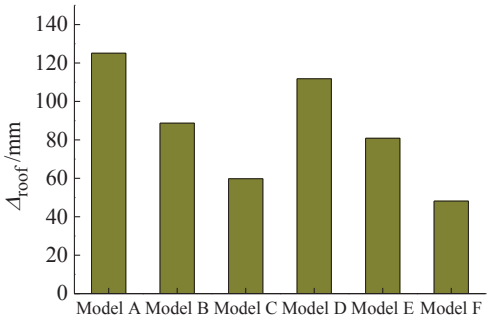

(b)

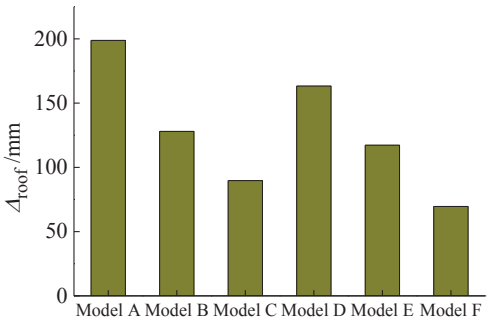

(c)

Fig 12

Click here to download Figure Fig 12.pdf

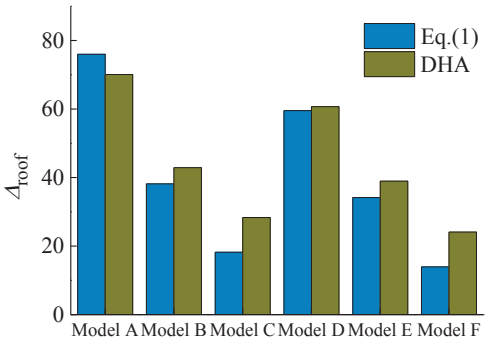

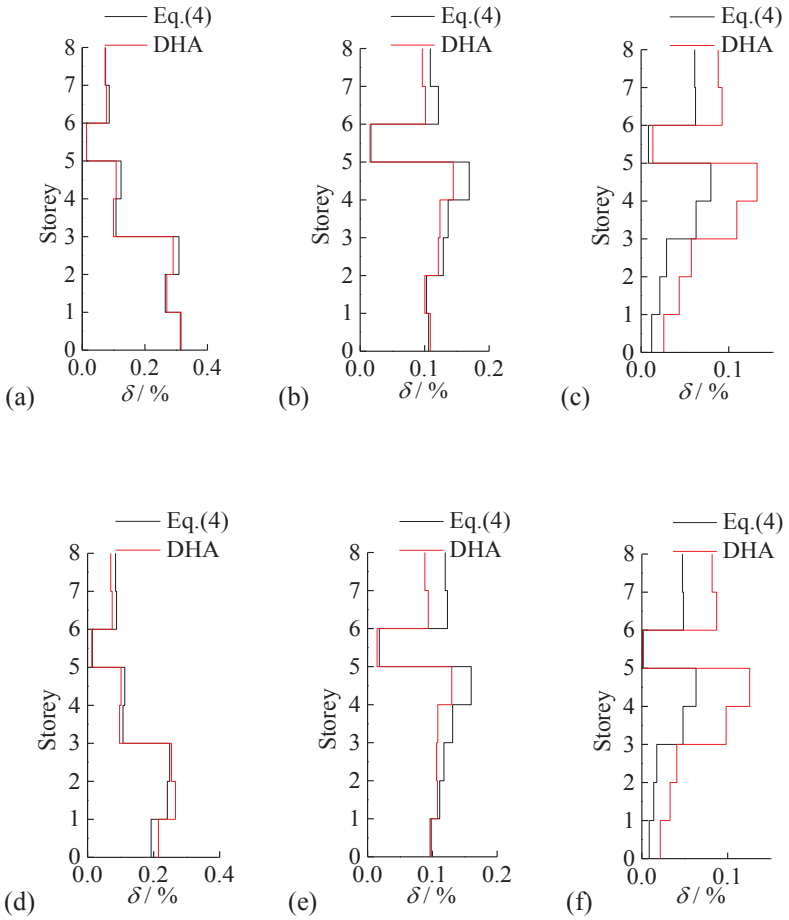

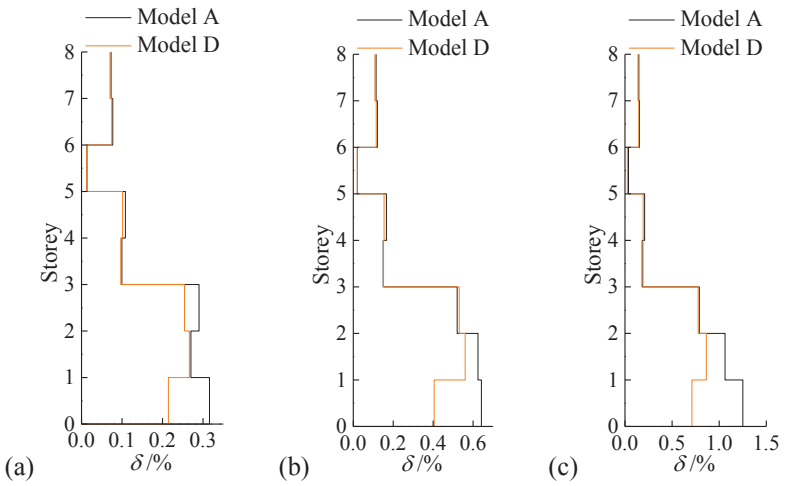

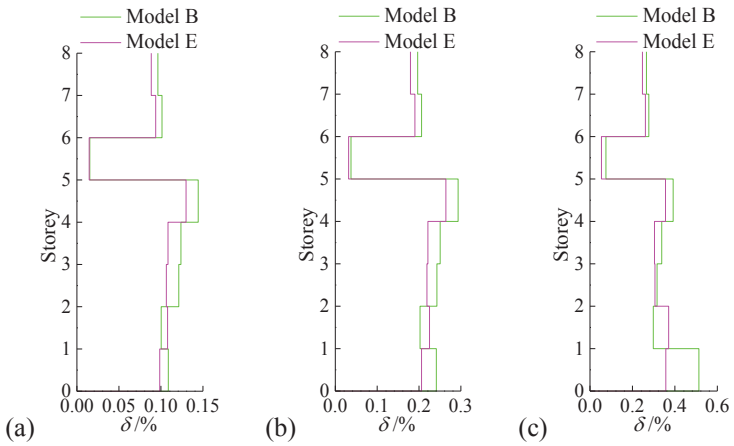

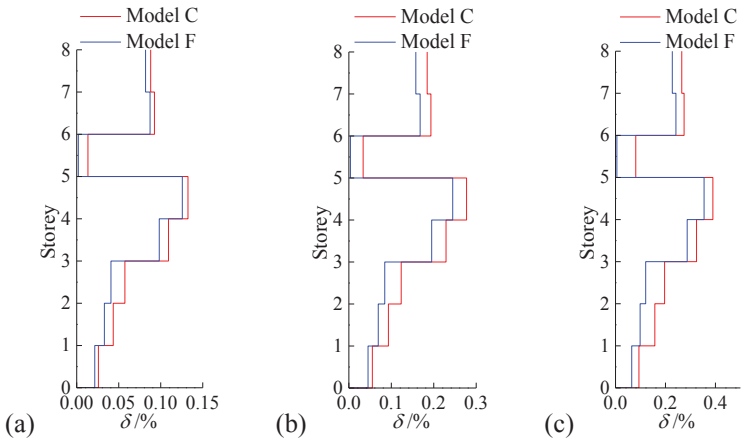

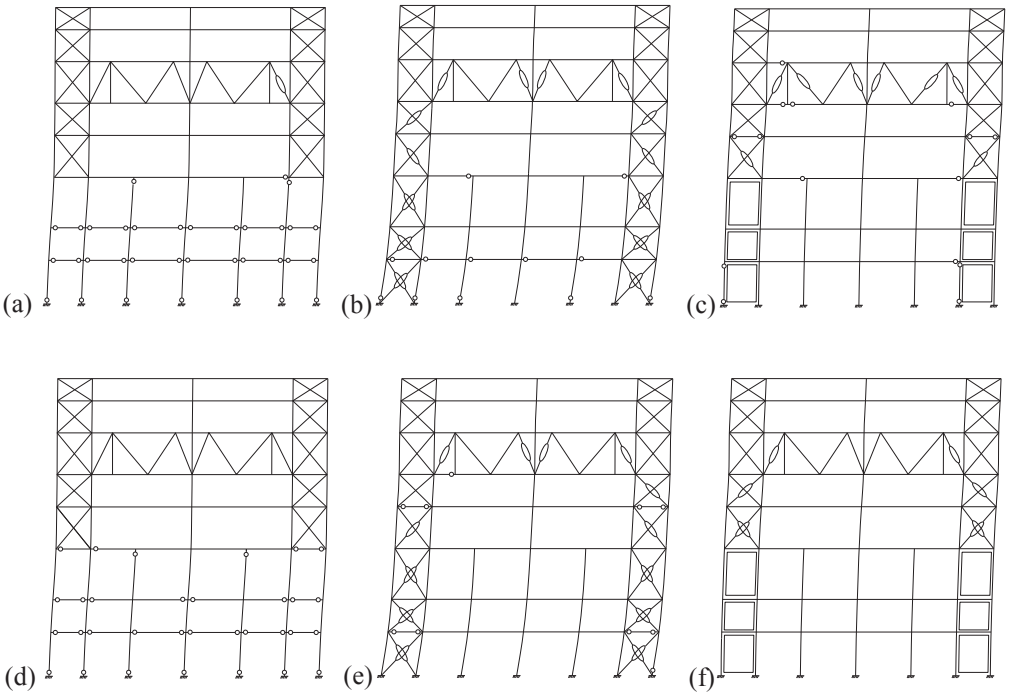

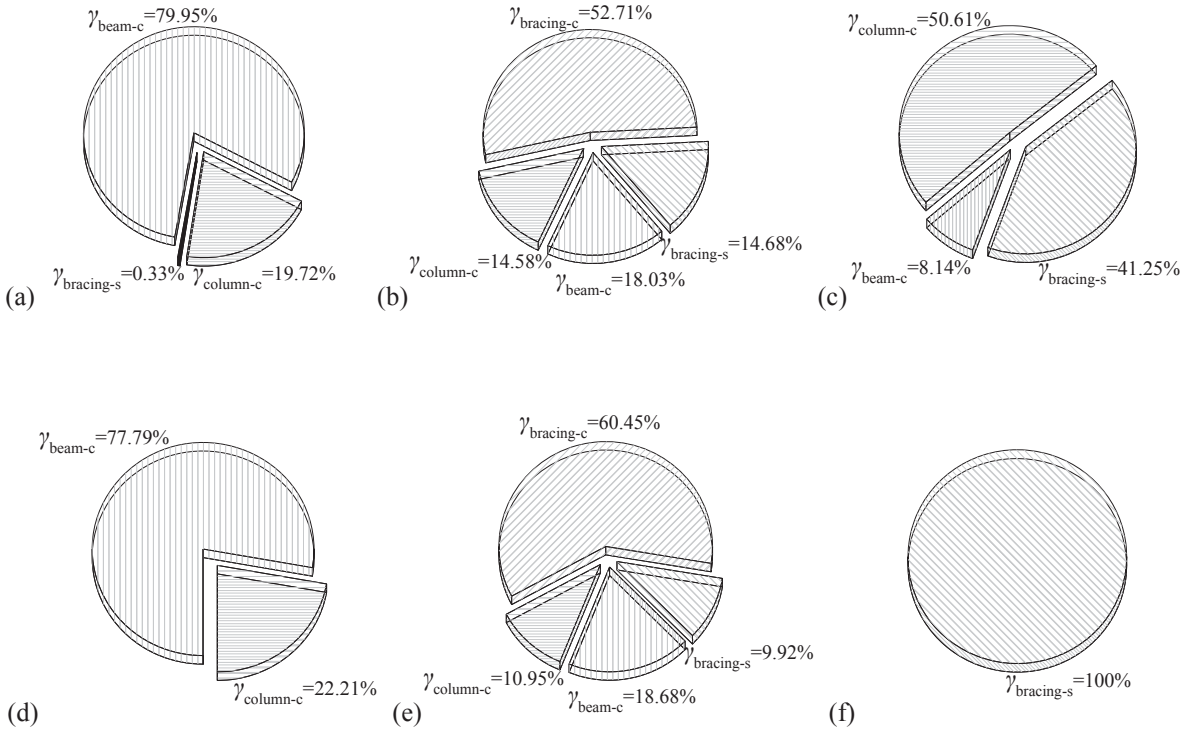

Fig 19

Click here to download Figure Fig 19.pdf

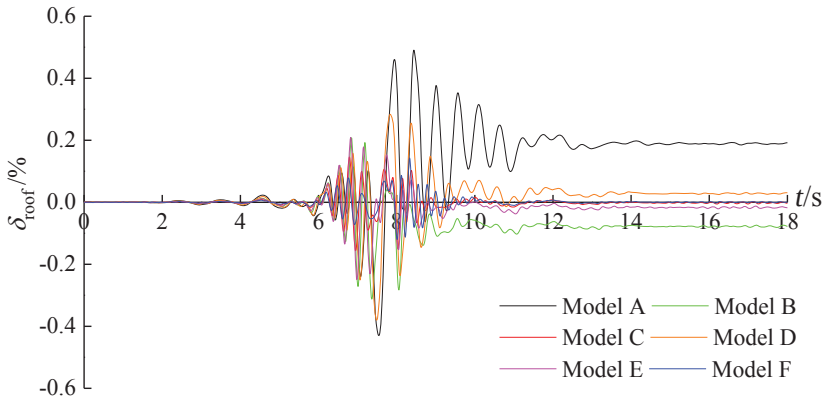

List of Figure Captions

Fig.1. Example projects of RC-steel hybrid frames: (a) Wenzhou Power-generation Plant; and (b) Jiangyou Power-generation plant.

Fig.2. Elevation of structure: (a) Pre-existing RC frame; and (b) Reconstructed hybrid frame.

Fig.3. Details of strengthening methods: (a) Local strengthening on components; and (b) Bracing connection scheme.

Fig.4. Enhancement of strength of RC beams and columns before and after strengthening: (a) Moment(M) vs. curvature(C) of RC beam; and (b) Axial force(N)-moment(M) curve of RC column.

Fig.5. Finite element model and stress distributions of RC beam-column joint: (a) Finite element model; (b) Stress distribution in concrete; (c) Stress distribution in rebars; (d) Stress distribution in angle steels and steel batten plates; and (e) Stress distribution in steel plates.

Fig.6. Six variants of retrofitted structure: (a) Model A; (b) Model B; (c) Model C; (d) Model D; (e) Model E; and (f) Model F.

Fig.7. Values of $\overline{\beta}_i$ coefficient for six hybrid frames: (a) Model A; (b) Model B; (c) Model C; (d) Model D; (e) Model E; and (f) Model F.

Fig.8. Characterisation of components modelling: (a) Chord rotation model; (b) Force-deformation relationship; and (c) Stiffness degradation parameters.

Fig.9. Target design spectrums.

Fig.10. Comparison of target design spectra and matched response spectra of input ground motions: (a) PGA=0.4g; (b) PGA=0.8g; and (c) PGA=1.2g.

Fig.11. Roof displacements of six models: (a) PGA=0.4g; (b) PGA=0.8g; and (c) PGA=1.2g.

Fig.12. Comparison of roof displacements between Eq. (1) and dynamic time-history analysis.

Fig.13. Comparison of story drift ratio between Eq.(4) and dynamic time-history analysis: (a) Model A; (b) Model B; (c) Model C; (d) Model D; (e) Model E; and (f) Model F.

Fig.14. Story drift ratios of Model A and Model D: (a) PGA=0.4g; (b) PGA=0.8g; and (c) PGA=1.2g.

Fig.15. Story drift ratios of Model B and Model E: (a) PGA=0.4g; (b) PGA=0.8g; and (c) PGA=1.2g.

Fig.16. Story drift ratios of Model C and Model F: (a) PGA=0.4g; (b) PGA=0.8g; and (c) PGA=1.2g.

Fig.17. Plastic hinge distribution patterns of six models: (a) Model A; (b) Model B; (c) Model C; (d) Model D; (e) Model E; and (f) Model F.

Fig.18. Hysteretic energy dissipation participation factors of primary components: (a) Model A; (b) Model B; (c) Model C; (d) Model D; (e) Model E; and (f) Model F.

Fig.19. Roof drift ratios of six models.